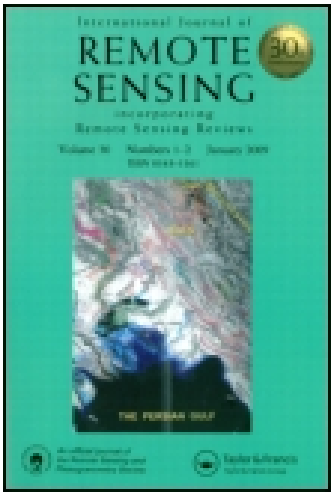

International Journal of Remote Sensing
Publication details, including instructions for authors and subscription information:
http://www.tandfonline.com/loi/tres20

Dye concentration estimation by remotely-sensed spectral radiometry

O. ZALLOUM [a], E. O' MONGAIN [a], J. WALSH [a], S. DANAHER [b] & L. STAPLETON [c]

[a] Physics Department, University College, Stillorgan Road, Dublin, 4, Ireland

[b] Faculty of Information and Engineering Systems, Leeds Metropolitan University, Leeds, England, LS1 3HE, U.K.

[c] Environmental Research Unit, St. Martin's House, Waterloo Road, Dublin, 4, Ireland

Published online: 07 May 2007.

To cite this article: O. ZALLOUM, E. O' MONGAIN, J. WALSH, S. DANAHER & L. STAPLETON (1993) Dye concentration estimation by remotely-sensed spectral radiometry, International Journal of Remote Sensing, 14:12, 2285-2300, DOI: 10.1080/01431169308954037

To link to this article: http://dx.doi.org/10.1080/01431169308954037

INT. J. REMOTE SENSING, 1993, VOL. 14, NO. 12, 2285–2300

Dye concentration estimation by remotely-sensed spectral radiometry

O. ZALLOUM, E. O' MONGAIN, J. WALSH
Physics Department, University College, Stillorgan Road, Dublin 4, Ireland

S. DANAHER
Faculty of Information and Engineering Systems,
Leeds Metropolitan University, Leeds LS1 3HE, England, U.K.

and L. STAPLETON
Environmental Research Unit, St. Martin's House, Waterloo Road, Dublin 4, Ireland

(Received 25 November 1991; in final form 5 December 1992)

Abstract. The results of a study aimed at the determination of the concentration of Rhodamine-B dye at parts per billion (ppb) levels from remotely-sensed optical reflectance spectra of marine and fresh water are described. An estimated signal is derived from spectral radiometer data using an improved cross correlation technique. In applying this technique use is made of the fact that some *a priori* information is available regarding the spectral distribution of the signal produced by the dye. The procedure for calibrating the signal estimate with ground truth data is described.

1. Introduction

Tracing the concentration of natural or introduced materials is a method for studying mixing rates and movements within water-bodies, particularly in cases where marine or estuarine waters are used for the controlled disposal of treated effluents. The patterns of dye dispersion have been mapped by single or multi-band aerial photography as an alternative to *in situ* sampling or flourometry (e.g., Valerio and Llebaria 1982, Wilkinson and Curran 1985 and Citeau and Noel 1980). Danaher *et al.* 1992 have demonstrated the limited ability of such single-band or multi-band radiometry to discriminate against background variations and noise under certain simple data inversion strategies. A method of airborne dye tracing, providing calibrated quantitative information on the dye concentration, is described here. An airborne spectral radiometer was used to measure spectral signatures over a water body, in regions with and without dye; a limited number of *in situ* dye concentration samples were required, together with a laboratory measurement of the spectral characteristic of the dye.

The concentrations of the *in situ* samples are used as a calibration data set to estimate the parameters of an algorithm which yields quantitative estimates of dye concentrations from the spectral radiometer measurements. The calibrated algorithm can then be applied to all the radiometer measurements, providing a remotely sensed concentration mapping capability.

0143–1161/93 $10.00

2. Method

Rhodamine-B is one of the dyes generally recommended for time of travel and dispersion measurements. Its strong orange fluorescence in weak solutions is easily isolated and detected. It is soluble, harmless in low concentrations, inexpensive, reasonably stable and easily identifiable against the background.

The water body being assessed may contain not only the fluorescent dye, but also large quantities of microscopic algae, dissolved and particulate organic material, and inorganic sediment mixed throughout the water body. These, together with atmospheric absorption and scattering and with the effects of the instrument profile and bottom reflections, will interfere with and mask the desired spectral distribution from which the dye concentration is to be estimated.

The principal advantages of the method described below include the facts that: (*a*) no subjective preselection of bands is required for high signal-to-noise ratio; (*b*) it results in excellent sensitivity; (*c*) it has the ability to quantify accurately and to subtract unwanted background; and (*d*) the detailed spectra obtained provide an excellent data base for simulation studies to assist in the design of future satellites and airborne dye tracing instruments.

2.1. *The observed spectra*

Suppose that the reflectance spectrum or the upwelling radiance spectrum is measured in n spectral bands over m different locations. These remotely-sensed observations can then be represented by the m-row n-column matrix $\mathbf{O}$. It is further supposed that a subset m_1 of the observed spectra are obtained over the water body in positions or at times when there is no dye present. Finally a small number m_2 of the m-m_1 observations will contain dye signal which can be related to corresponding ground measurements of the dye concentration for calibration purposes.

The observed spectral radiance $\mathbf{O}$ may be considered to be composed of the sum of Signal(Dye) $\mathbf{S}$, Background $\mathbf{B}$, and noise $\mathbf{N}$, contributions, i.e.,

$$\mathbf{O}=\mathbf{S}+\mathbf{B}+\mathbf{N} \tag{1}$$

where $\mathbf{O}$ is the m-row n-column observation matrix. It is required to produce an estimate of the signal strength in each observation of $\mathbf{O}$, independent of the contribution of the background and noise.

The noise $\mathbf{N}$ is instrumental and, apart from the blue region of the spectrum (where the responsivity of the charge coupled sensing device, CCD, is low), it does not dominate. The variations in the background, as a result of constituent changes in the water, of surface reflectance, and of variations in illumination conditions, are the dominant features of the spectra.

The improved cross-correlation algorithm (ICCA) (Danaher *et al.* 1992) processes $\mathbf{O}$ and produces a scalar estimate of the signal intensity, $\mathbf{I}$, which is related to the magnitude of $\mathbf{S}$ in the observed spectra. The technique is of greatest use when a known signal is to be detected in the presence of both noise and background variations. The procedure involves the following steps:

2.1.1. *Background model*

The m_1 observations within $\mathbf{O}$ are used to create a characteristic vector model of the background variations. This technique attempts to reduce the number of parameters defining the background and expressing it as a mean background $\bar{\mathbf{B}}$ plus a number of orthogonal unit vectors $\mathbf{v}_i$ times their scalar multipliers $\mathbf{w}_i$ (see for

example Simonds 1963 or Gower *et al.* 1984). This is achieved by finding the characteristic vectors (eigenvectors) of the covariance matrix of a population of background spectra without signal S. Provided the background model is applicable over all the regions of observations, the observed spectra can be written as:

$$\mathbf{O}=\mathbf{S}+[\bar{\mathbf{B}}+\mathbf{w}_1\mathbf{v}_1+\mathbf{w}_2\mathbf{v}_2+\cdots\mathbf{w}_n\mathbf{v}_n]+\mathbf{N} \tag{2}$$

where $\bar{\mathbf{B}}$ is the mean background, $\mathbf{v}_i$ are the characteristic unit row vectors of dimension n and $\mathbf{w}_i$ are scalar multipliers (arranged in the form of column vectors of dimension m). Generally it is found for remote sensing data that nearly all the variation in the background can be explained by the first few characteristic vectors. The series is thus truncated after the pth term. For 50 spectral points ($n=50$) p will be typically about 4. The first few characteristic unit row vectors $\mathbf{v}_i$ will be used in deriving the key spectrum.

2.1.2. *Key spectrum*

The *a priori* information concerning the spectral shape of **S** can be described by a unit spectral vector **r** of dimension n. This reference spectrum **r** may be produced in the laboratory under ideal conditions (§3.2 below). It is now necessary to search the observation matrix **O** for components of the reference spectrum **r** which are orthogonal to the background vectors $\mathbf{v}_i$.

A key vector **k** is constructed from **r** by removing the components of the vector **r** in the direction of $\mathbf{v}_1, \mathbf{v}_2, \mathbf{v}_3 \ldots \mathbf{v}_p$ and renormalizing to a unit vector. This is achieved as follows:

Let
$$\mathbf{k}_1 = \mathbf{r}$$
$$\mathbf{k}_2 = \mathbf{k}_1-(\mathbf{k}_1\cdot\mathbf{v}_1)\mathbf{v}_1$$

where the product $(\mathbf{k}_1\cdot\mathbf{v}_1)$ is a scalar product and $(\mathbf{k}_1\cdot\mathbf{v}_1)\mathbf{v}_1$ gives a column vector of dimension n.

$$\mathbf{k}_3 = \mathbf{k}_2-(\mathbf{k}_2\cdot\mathbf{v}_2)\mathbf{v}_2$$
$$\vdots$$
$$\mathbf{k}_{p+1}=\mathbf{k}_p-(\mathbf{k}_p\cdot\mathbf{v}_p)\mathbf{v}_p$$
$$\mathbf{k} = (\mathbf{k}_{e+1})(|\mathbf{k}_{e+1}|)$$

This process is illustrated in §5 and figure 7.

2.1.3. *Signal estimation*

The signal estimate I is defined by

$$\mathbf{I}=(\mathbf{O}-\bar{\mathbf{B}})\mathbf{k} \tag{4}$$

where **k** is the unitised column vector from above. I has m elements; of these, the elements corresponding to the m_1 background spectra should approximate to zero. Indeed this test for zero estimate can be used in regions without dye as a test of the effectiveness of the technique in removing background and noise effects. As noted by Danaher *et al.* (1992) the ability of correlation techniques to discriminate over noise is generally quite good; noise components should be equally distributed in all directions in n dimensional spectral space.

2.1.4. *Calibration*

The set of estimates in I can be converted to a set of concentrations C by using the m_2 ground truth samples to fit a calibration function. Absorption and scattering coefficients are proportional to concentration. The calibration relation is generally well described by an exponential function with some constraints.

3. Measurements

3.1. *Airborne spectral data*

Nineteen flight lines (runs) of spectral data were taken on two different days as follows:

3 July 1990	3 flights	11 flight lines
16 July 1990	3 flights	8 flight lines.

All flight data sets consisted of the sea surface spectral radiance matrix $\mathbf{O}_r$ and sky irradiance matrix $\mathbf{O}_{ir}$ obtained using a 2-channel CCD spectral radiometer built at University College Dublin (Walsh 1987). The instrument was mounted in a light aircraft operating at a height of about 450 m. As a regular check on the instrument a series of calibration measurements, with the down-looking channel fibre optic probe measuring reflected radiance from a standard grey card reflector and the uplooking channel probe continuing to measure sky irradiance, was made before and after every flight. For the wavelength range of 400–900 nm, a 1-row 50-column array **Cf** of calibration factors was obtained

$$\mathbf{Cf}_{(j)} = \bar{\mathbf{O}}_{u_j} \bar{\mathbf{O}}_{d_{(j)}} \tag{5}$$

where j represents the spectral bands in the spectrometer; $j = 1, 2, 3, \ldots, 50$,

$\bar{\mathbf{O}}_u \equiv$ column mean reflected radiance from the grey card (upwelling radiance), and

$\bar{\mathbf{O}}_d \equiv$ column mean irradiance (downwelling irradiance).

The spectral relative reflectance $\mathbf{O}_F$, for each flight run was then calculated using the expression

$$\mathbf{O}_{F_{(i,j)}} = \left[\frac{\mathbf{O}_{r_{(i,j)}}}{\mathbf{O}_{ir_{(i,j)}}} \right] \mathbf{Cf}_{(j)} \tag{6}$$

where $\mathbf{O}_r \equiv$ the spectral radiance from dye targets, $\mathbf{O}_{ir} \equiv$ sky irradiance. The left-hand matrix is a family of curves with m rows corresponding to position along a flight run and $n (= 50)$ columns corresponding to the wavelength bands in the range 400 to 900 nm. $i \equiv 1, 2, 3, \ldots, m$ for m observations, and $j \equiv 1, 2, 3, \ldots, n$ for n spectral bands.

Figure 1 shows a typical spectral relative reflectance data matrix with mean background spectra subtracted, $(\mathbf{O}_F - \bar{\mathbf{B}})$, for a flight run. The mean background spectra, $\bar{\mathbf{B}}$, (see §4 background analysis, below), is shown by the solid-circle line-type.

3.2. *Reference spectrum determination*

To determine a suitable reference spectrum for the dye, measurements of the spectral radiance from diluted dye solutions and of a spectrally flat standard grey card reflector were made alternately in the laboratory using the same spectral radiometer. The dye solutions were measured in 25 l containers with black walls and bottom.

The laboratory data sets included data taken for five different dye concentrations (figure 2). The matrix of upwelling radiances from the dye and from the grey card were used to form m-row n-column data matrices $\mathbf{O}_L$ and $\mathbf{O}_G$ respectively, with $m > n$.

Although not essential for this analysis, another data set was gathered for instrument profile correction. This data set was composed of $\mathbf{O}_{G1}$ and $\mathbf{O}_{G2}$ which were taken over the grey card reflector with the channels used to measure $\mathbf{O}_L$ and $\mathbf{O}_G$ respectively. The dye relative reflectance was calculated from

$$\mathbf{O}_{D_{(i,j)}} = \left[\frac{\mathbf{O}_{L_{(i,j)}}}{\mathbf{O}_{G_{(i,j)}}}\right]\left[\frac{\bar{\mathbf{O}}_{G2_{(j)}}}{\bar{\mathbf{O}}_{G1_{(j)}}}\right] \tag{7}$$

where $\bar{\mathbf{O}}_{G1}$ and $\bar{\mathbf{O}}_{G2}$ are the column means of $\mathbf{O}_{G1}$ and $\mathbf{O}_{G2}$ respectively.

The dc variation of each spectrum in $\mathbf{O}_L$ was removed by subtracting the row mean from each column in $\mathbf{O}_L$. The resultant matrix was further corrected by subtraction of the mean spectrum (column mean subtraction) before characteristic vector analysis was applied to determine a suitable reference spectrum. The resulting eigenvectors of the covariance matrix were normalised to unity. The ratio of the ith eigenvalue to the sum of all the eigenvalues is a measure of the percentage of the original data variance which is explained by the ith eigenvector. The first eigenvector contributed to 67 per cent of the variance in the dye concentration data (figure 3). This vector was taken as a reference spectrum $\mathbf{r}$.

3.3. *Ground truth data collection*

Ground truth campaigns were undertaken by the Environmental Research Unit of the Irish Department of Environment on 3 and 16 July 1990. On each occasion 140 l of dye solution were released at the sewage outfall at Ringsend, Dublin Bay, Ireland. Boats were used to sample at a number of stations. Dye concentration contour maps were estimated from this ground data, supplemented by image processing of black and white aerial photographs taken using a red filter. A typical contour plot and corresponding flight track are shown in figure 4.

4. Background analysis

Background spectra away from the dye plume were noted and extracted from the corrected flight data (6); these represented the m_1 background observations referred to in §2.1. above.

These chosen background scans from the first five runs of 3 July were combined to form a 89 by 50 background matrix for day one, $\mathbf{B}_1$. Background scans from five other runs of 16 July formed a 78 by 50 background matrix for day two, $\mathbf{B}_2$ (figure 5). The considerable variability in the background data and the difference in spectral shape between the two day's data are due to a combination of factors; the raw data correction procedure differed on the two days, the illumination conditions were more variable due to cloud cover variability on day two and the two sets of data could have contained spectra over different conditions of sediment concentration and different bottom reflection conditions.

Characteristic vector analysis was undertaken for each background data set after dc removal and mean spectrum subtraction as described in §3.2.

Nearly all the variations were explained by four characteristic vectors in each background data matrix (figure 6). The unit eigenvectors $\mathbf{v}_1, \mathbf{v}_2, \mathbf{v}_3$, and $\mathbf{v}_4$ for day

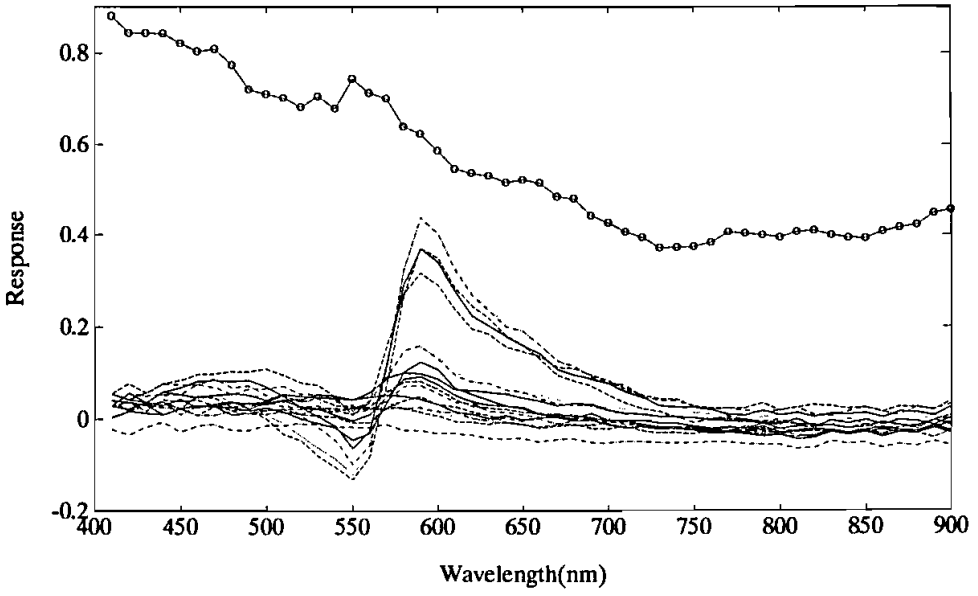

(*a*)

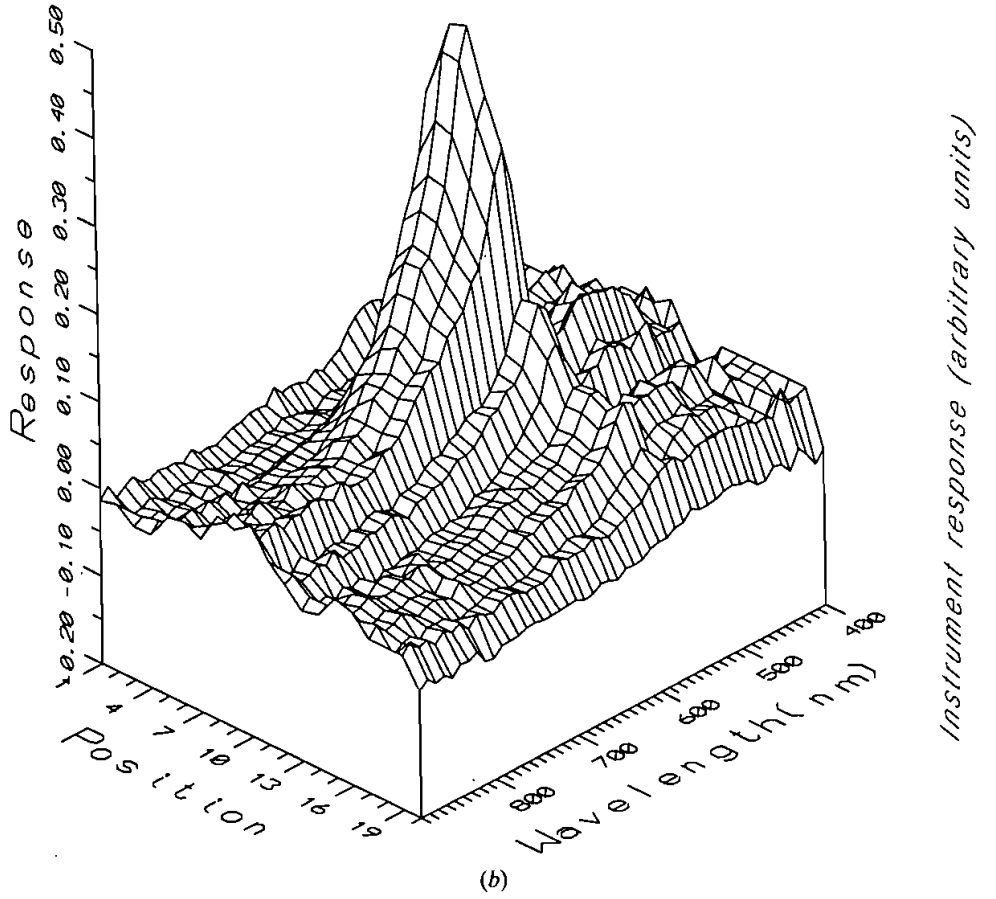

(*b*)

one and for day two were used to remove components of the reference spectrum that are parallel to these dominant characteristic vectors of $\mathbf{B}_1$ and $\mathbf{B}_2$ respectively (see below). It should be noted that these eigenvectors only represent the co-ordinate axes for a suitable model of the background; the individual vectors do not have any particular physical significance. The mean background $\bar{\mathbf{B}}_1$ and $\bar{\mathbf{B}}_2$ for each day was also determined.

5. Key spectrum determination

The reference spectrum $\mathbf{r}$ was orthogonalised to the background characteristic vectors of the two covariance background matrices $\mathbf{B}_1$ and $\mathbf{B}_2$ as described in § 2.1.2. to yield the key vectors for day one to two, $\mathbf{k}_1$ and $\mathbf{k}_2$, respectively. The process of orthogonalising the reference vector is described graphically in figure 7.

6. Signal determination

The signal estimates were then obtained from

$$I_1 = (\mathbf{O}_F - \bar{\mathbf{B}}_1)\mathbf{k}_1 \text{ for day one flights.}$$
$$I_2 = (\mathbf{O}_F - \bar{\mathbf{B}}_2)\mathbf{k}_2 \text{ for day two flights.} \quad (8)$$

Examples of scans across the dye plume are shown in figure 8. Note the absence of signal outside the plumes where the background has been effectively removed. These linear estimates of signal intensity now require calibration.

7. Signal calibration

Laboratory experiments in agreement with the literature (for example, Weidemann 1974) indicate that fluorescence intensity does not rise linearly with the dye's concentration. This fact is inherent in any irradiation/emission system, because both incident and emitted radiation are absorbed exponentially with depth. Although at very low concentrations the fluorescence seemed to increase linearly with increasing concentration, the slope becomes smaller at higher concentrations eventually inverting to a decrease at very high concentrations; the increasing absorption of the exciting and fluorescent light by the highly coloured water overwhelms the increase in fluorescence.

An algorithm to relate signal intensity to dye concentration was chosen for our analysis such that it provided for zero intensity at zero concentration and for the saturation effect that is observed at high concentrations. The form of this function is given by:

$$\mathbf{C} = K_1 ln(1 - I/K_2)) \quad (9)$$

Figure 1. (*a*) The response plotted is the difference between the typical relative spectral reflectance (equation (6)), $\mathbf{O}_F$, and $\mathbf{B}_2$, the mean background spectra for a flight run on 16 July 1990, day two. The mean background spectrum, is shown by the solid-circle line-type. Twenty spectral measurements (curves) were made in this particular flight run (scan). (*b*) is an orthographic plot of the relative reflectance spectra shown in (*a*). The plot is rotated through 45° around the response axis for clarity. The position axis represents the location of the observation (spectral measurement) in arbitrary units along the flight run.

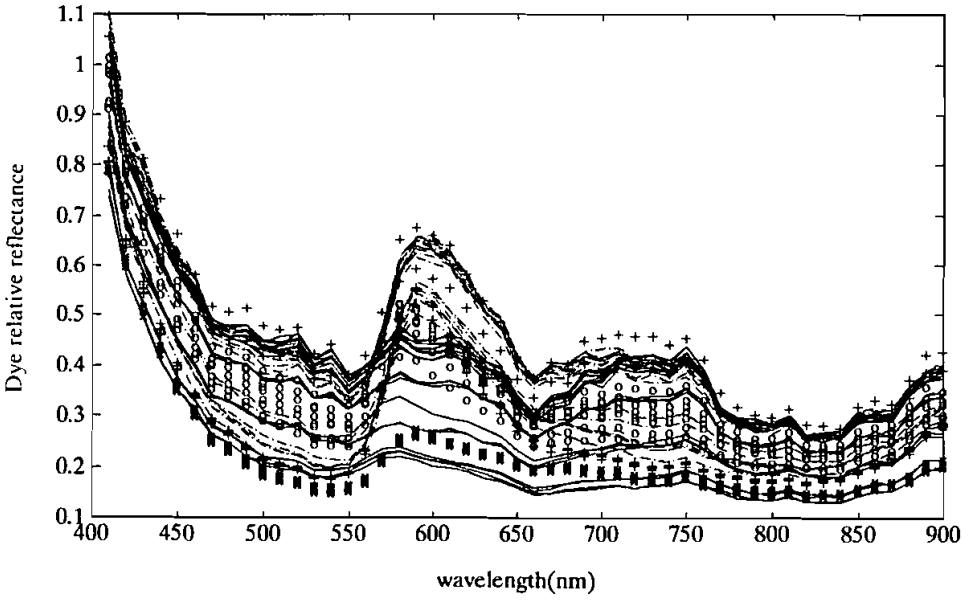

Figure 2. Dye relative reflectance (equation (7)). The spectral measurements (curves) were carried out in the laboratory for reference spectrum determination. Five different families of spectra are shown, representing five different dye concentrations. The increase in reflectance beyond $\lambda = 800$ nm, although the absorption of pure water increases, is thought to be related to the presence of Rhodamine B in the water.

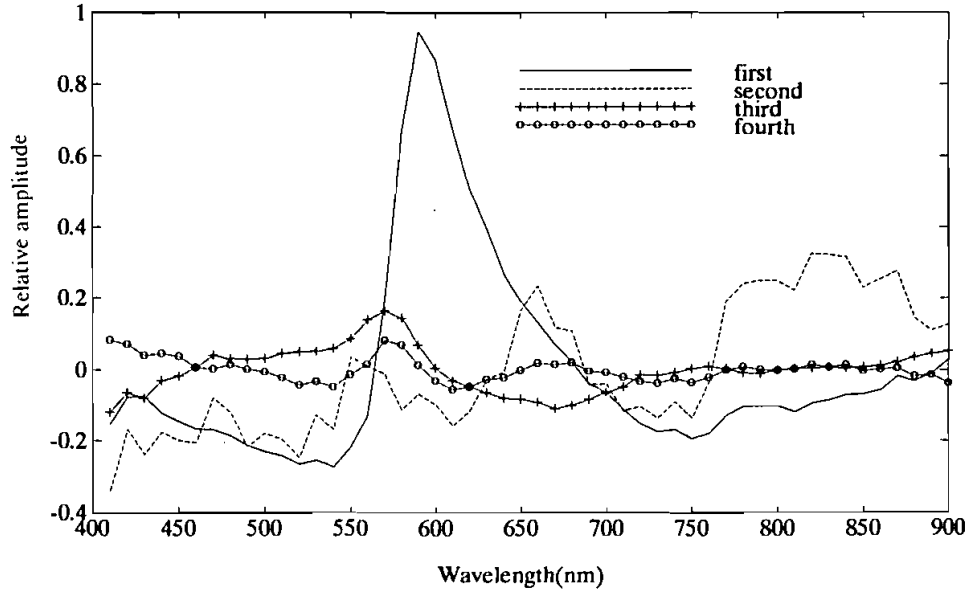

Figure 3. The first four characteristic vectors of the dye relative reflectance data of figure 2. The first vector explains most of the variation in the data, and was taken as the reference spectrum.

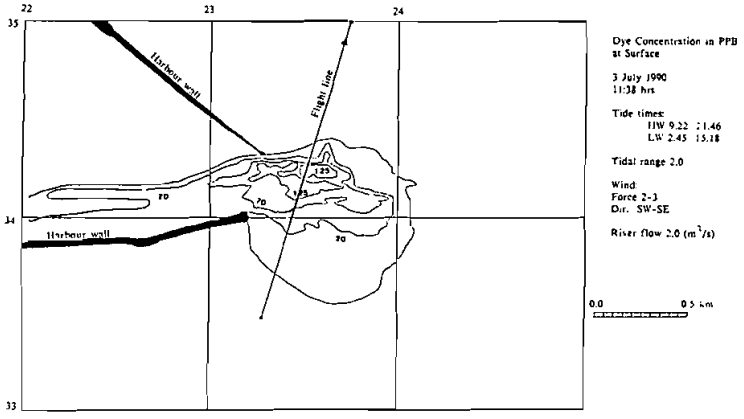

Figure 4. Typical contour map and a corresponding flight run. The dye plume peak is expected between measurement positions 7 and 8.

where C is the dye concentration in ppb and I is the intensity. This is not necessarily the only or best function for this purpose; however a considerably larger body of calibration data would be required to find the optimum function. Selecting data obtained at an altitude of about 450 m and over a range of relatively high values of known concentration (in the range 55 to 125 ppb) the constants K_1 and K_2 were determined. The values which gave the best fit over this range as determined using the Nelder-Meade simplex algorithm were $K_1 = -61{\cdot}3048$ and $K_2 = 0{\cdot}7443$. Aside from concentration, the constants K_1 and K_2 may also be sensitive to sample temperature, salinity, photochemical decay and fluorescence quenching factors.

The calibrated algorithm was then tested by using it to estimate the dye concentration at other locations where ground truth was available. The concentration values of these test points ranged from 1 to 60 ppb. A scatter plot of the estimated concentration Ce, versus ground truth concentration Cg is shown in figure 9. The rms error between Ce and Cg for these test points is $-12{\cdot}15$ dB (or 6·1 per cent), calculated from

$$\text{rms} = \sqrt{\Sigma_i [a_i - b_i]^2} \tag{10}$$

where

$$a_i = \frac{Ce_i - \overline{Ce}}{\sqrt{\Sigma_i [Ce_i - \overline{Ce}]^2}}$$

and

$$b_i = \frac{Cg_i - \overline{Cg}}{\sqrt{\Sigma_i [Cg_i - \overline{Cg}]^2}}$$

The correlation coefficient between Cg and Ce is 0·998.

7.1. *Calibration uncertainties*

Although a great deal of effort was exercised to ensure high reliability in ground truth measurements, their accuracy should not be overestimated; the difficulty of mapping the details of concentration distribution from sparse samples with sufficient

accuracy over large areas is obvious. The ground truth sampling used was of the surface concentration; samples were also obtained at 1 m depth, 3 m depth, mid-depth and from near bottom. Some combination of these may be better correlated with the integrated effect detected by the remote sensing radiometer. More calibration data would certainly improve the estimated concentration accuracy, and enable optimum calibration algorithms to be designed.

8. Typical scan profile

Figure 10 shows typical scan profiles across a flight run and shows the potential of the technique to provide estimates of dye concentration in regions without ground truth data. The absence of any signal estimates outside the main plume shows the power of the technique in discriminating against the background effects of sediment and bottom reflections which were present in the data, especially on day 2.

9. Alternative approach

As has been shown, the method used above is ideal for signal recovery of dyes or pollutants not normally present in the environment. In many cases however, it may

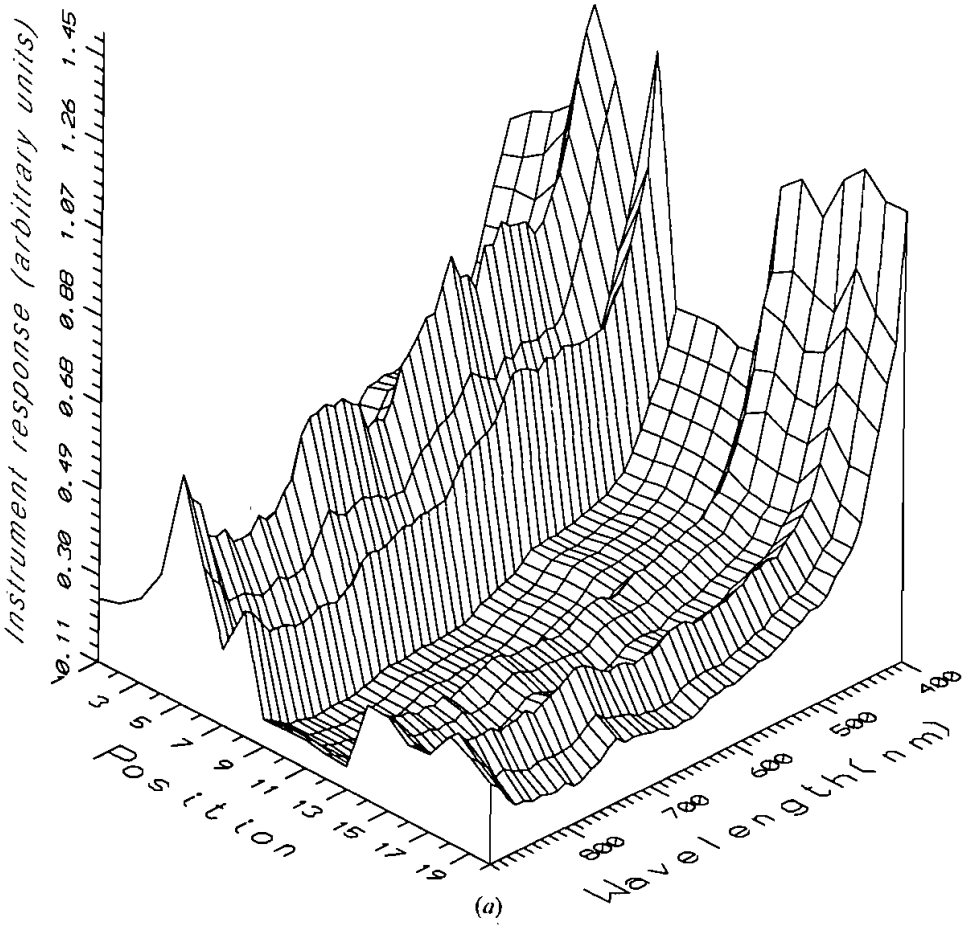

(a)

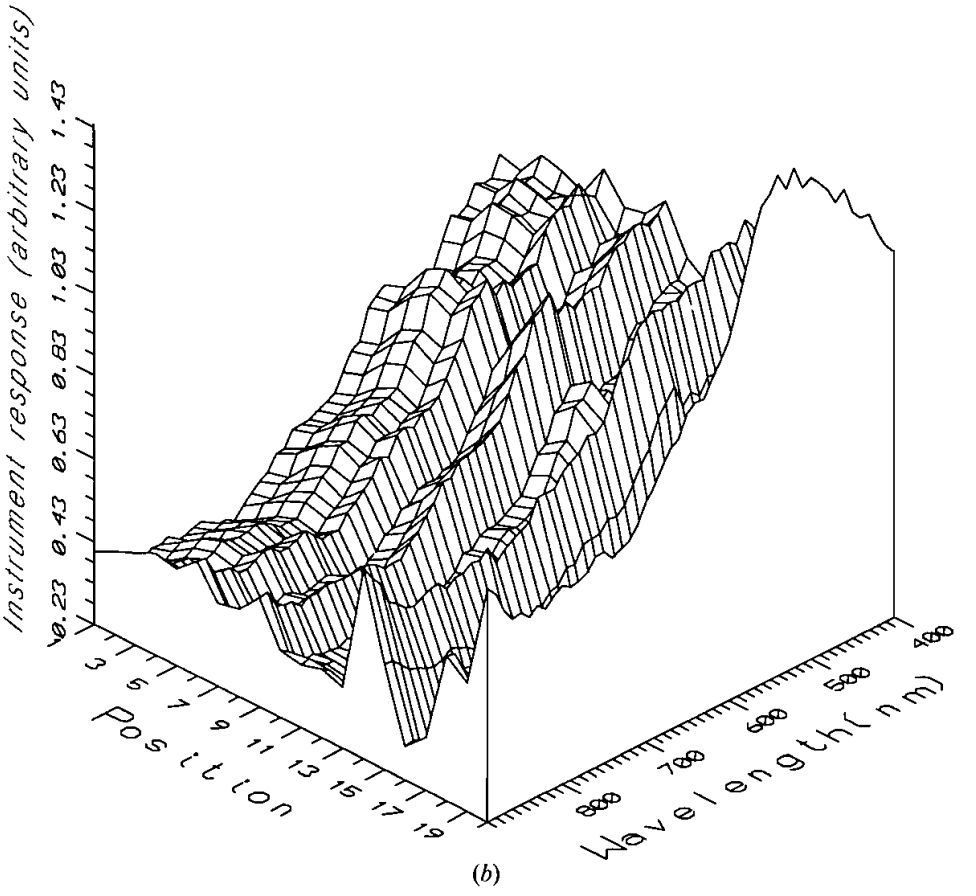

(*b*)

Figure 5. Orthographic representation of the first twenty background spectra. (*a*) from the 89 by 50 background matrix, $\mathbf{B}_1$, for day one flights. (*b*) from the 78 by 50 background matrix, $\mathbf{B}_2$, for day two flights. The plots are rotated through 45° around the response axis for clarity. The position axis represents the rows of the background matrix; i.e. location of the observation in the background matrix. The background matrices are extracted from the normalised flight data away from the dye plume.

be difficult to isolate signal and background; signal free samples of the background may not always be available. An alternative approach as described by Danaher and O'Mongain (1992) is available.

An algorithm using Singular Value Decomposition (SVD) can extract the key spectrum **k** from the observation data set in these circumstances. A set of calibration concentration values (A) is assumed to be available for a sizable set m_2 of spectral measurements **O**; unlike in § 2.1. above where the subset m_2 of calibration points was small. For these m_2 measurements, the key spectrum **k** must satisfy

$$\mathbf{A} = \mathbf{Ok}$$

or

$$\mathbf{A} = \mathbf{wlvk}$$

therefore

$$\mathbf{k} = \mathbf{v}^{-1}\mathbf{l}^{-1}\mathbf{w}^{-1}\mathbf{A} \qquad (11)$$

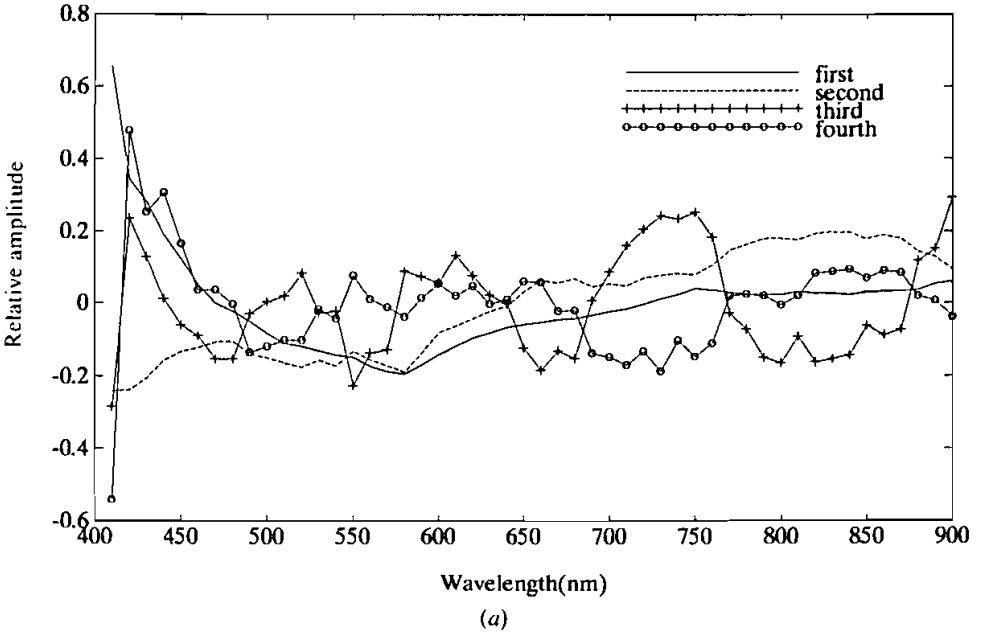

(*a*)

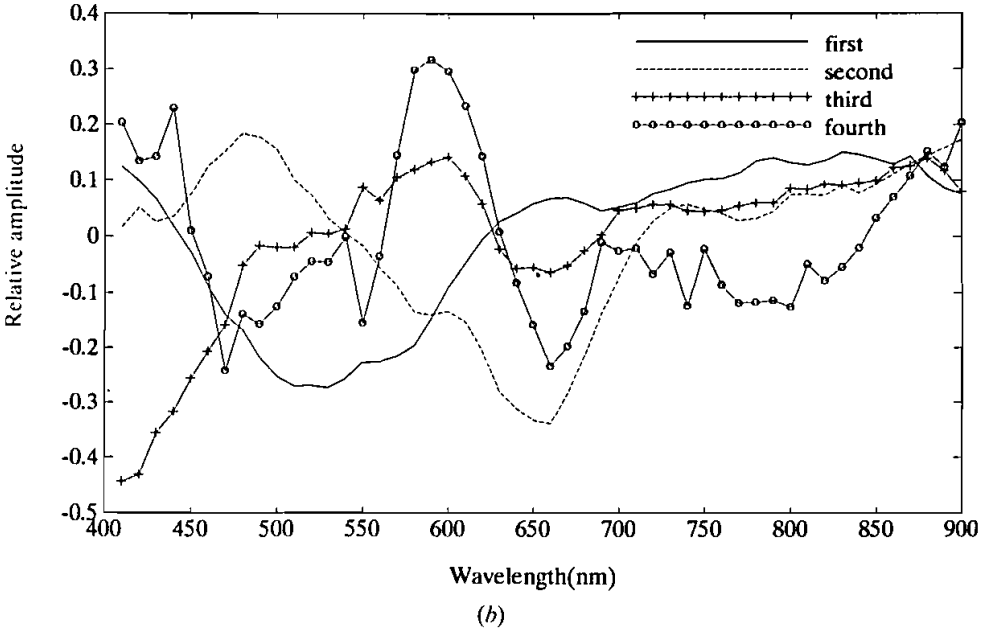

(*b*)

Figure 6. The first four characteristic vectors of background spectra away from the dye plume for (*a*) day one flights, and (*b*) day two flights.

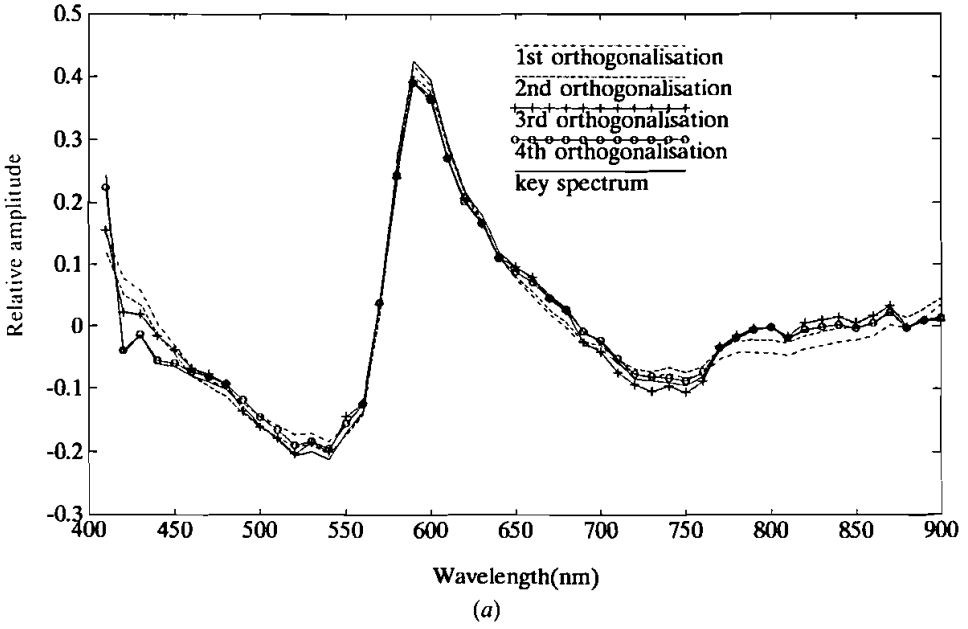

(*a*)

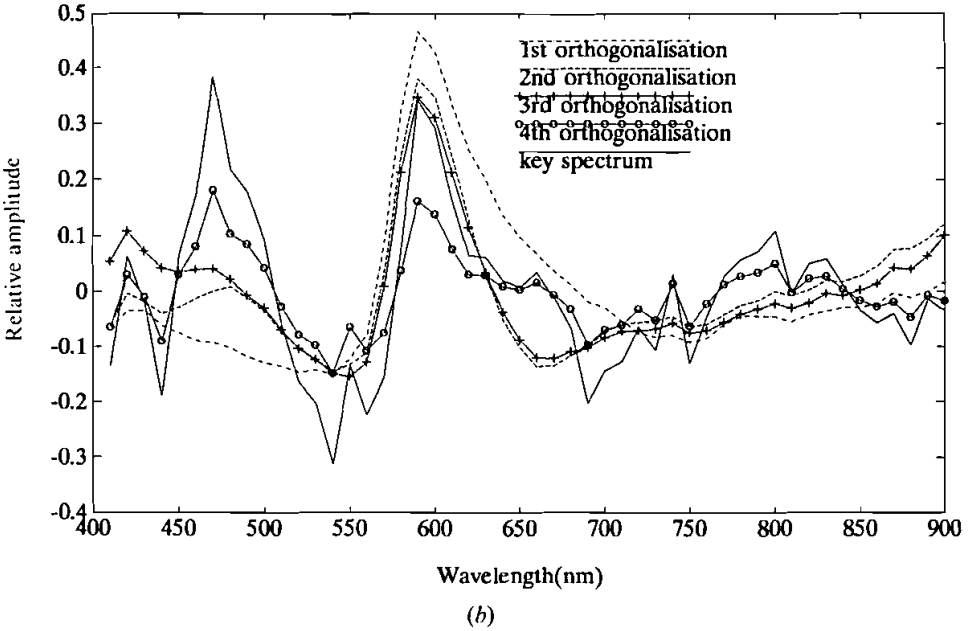

(*b*)

Figure 7. The process of removing the components of the reference spectrum that are parallel to the dominant characteristic vectors ($\mathbf{v}_1, \mathbf{v}_2, \mathbf{v}_3$, and $\mathbf{v}_4$) of background data (*a*) for day one flights, (*b*) for day two flights.

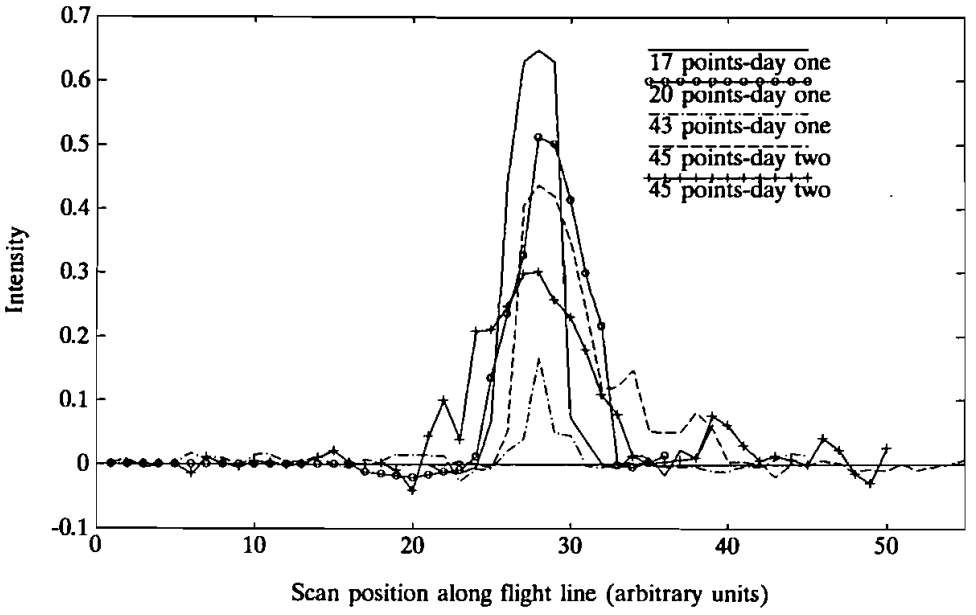

Figure 8. Plot of intensity I versus observation position along five typical flight runs.

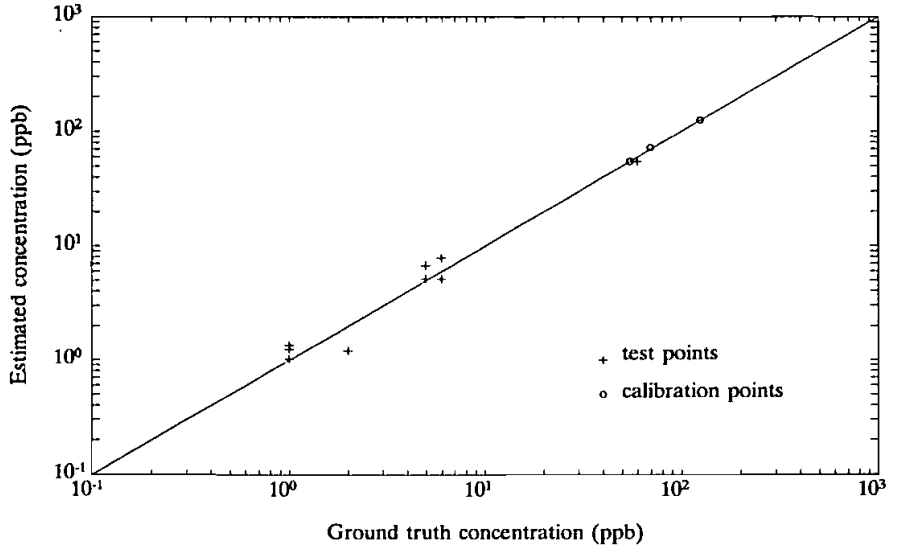

Figure 9. Logarithmic scatter plot of estimated concentration Ce versus ground concentration, Cg. The line represents the ideal case to show the accuracy of the algorithm in estimating Ce. The most accurate ground truth measurements were selected for calibration.

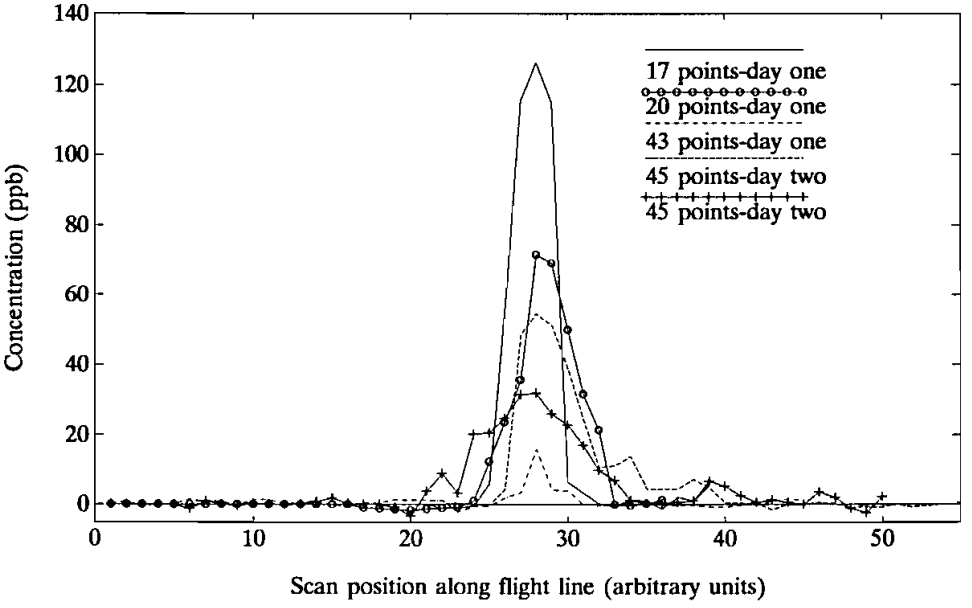

Figure 10. Estimated dye concentration (ppb) for the scans in figure 8.

where **wlv** is the SVD of **O** (see for example Marple 1987). The key spectrum **k** may then be used to determine **A** for the remaining population $m\text{-}m_2$ of **O** using $\mathbf{A}=\mathbf{Ok}$. The method is powerful and can be applied for any added or natural substance, but requires a larger calibration data set than was available in the work described above. Note, as both **v** and **w** are matrices containing orthonormal vectors, $\mathbf{v}^{-1}=\mathbf{v}^T, \mathbf{w}^{-1}=\mathbf{w}^T$. Also, as **l** is diagonal, $\mathbf{l}^{-1}$ can be obtained by taking the reciprocal of the diagonal terms.

10. Conclusions

The results obtained from the improved cross-correlation algorithm, indicate that rapid synoptic assessment of surface layer concentrations is feasible from passive spectral radiometers. In this study the minimum detectable level of dye concentration (the mean standard deviations of estimated dye concentrations outside the main plumes for five typical flight lines) was of the order of 1·5 ppb. Further, the ICCA, like cross-correlation algorithms, has the advantage that no *a priori* choice of spectral bands has to be made; and yet use is made of the *a priori* information regarding the predicted signal characteristics. The ICCA technique is linear and offers excellent background and noise suppression. Other algorithms such as band ratio and curvature algorithms suffer from non linearity, poor noise and background suppression (see for example, Danaher and O'Mongain 1992, Campbell and Esaias 1983). In addition, an *a priori* choice about which bands to use must be made. It is seldom clear how the optimum bands should be chosen. Further improvements in instrumentation and calibration processes may increase the sensitivity of this technique.

The technique can be applied to water constituents other than dye provided that a similar observation strategy can be realised; that regions with and without the desired constituent can be recognised and that sufficient spectral information regarding the optical effects of the constituents are known.

References

CAMPBELL, J. W., and ESAIAS, W. E., 1983, Basis for spectral curvature algorithms in remote sensing of chlorophyll. *Applied Optics*, **22,** 1084–1093.

CITEAU, J., and NOEL, J., 1980, A diffusing patch of rhodamine analysed by digitised aerial photography. *Coastal and Marine Applications of Remote Sensing*, edited by A. P. Cracknell, (Nottingham: Remote Sensing Society), pp. 21–24.

DANAHER, S., and O'MONGAIN, E., 1992, Singular value decomposition in multi-spectral radiometry. *International Journal of Remote Sensing*, **13,** 1771–1777.

DANAHER, S., O'MONGAIN, E., and WALSH, J., 1992, A new cross-correlation algorithm and the detection of Rhodamine-B dye in sea water. *International Journal of Remote Sensing*, **13,** 1743–1755.

GOWER, J. F. R., SIM, S., and BARSTAD, G. A., 1984, The information content of different spectral ranges for remote chlorophyll estimation in coastal waters. *International Journal of Remote Sensing*, **5,** 349–364.

MARPLE, S., 1987, *Digital Spectral Analysis with Applications.* (Englewood Cliffs, N.J.: Prentice Hall).

SIMONDS, J. L., 1963, Application of characteristic vector analysis to photographic and optical response data. *Journal of Optical Society of America*, **53,** 968–974.

VALERIO, C., and LLEBARIA, A., 1982, A quantitative analysis system for aerial photographs applied to coastal planning. *International Journal of Remote Sensing*, **3,** 181–197.

WALSH, J., 1987, *Development of Low Altitude Remote Sensing Spectrometer.* M.Sc. Thesis presented to The National University of Ireland.

WEIDEMANN, H., 1974, The use of fluorescent dyes for turbulence studies in the sea. In *Optical Aspects of Oceanography*, edited by N. G. Jerlov and E. Steemann Nielsen, (London: Academic Press Inc.), Chapter 12, pp. 257–288.

WILKINSON, W. B., and CURRAN, P. J., 1985, The use of aerial photography and image processing to measure dye dispersion from along sea outfall. *Proceedings of the Institution of Civil Engineers*, **79,** 327–348.